HHS Public Access

Author manuscript

Sens Actuators B Chem. Author manuscript; available in PMC 2020 May 11.

Published in final edited form as:

Sens Actuators B Chem. 2019 July 1; 290: 616–624. doi:10.1016/j.snb.2019.02.031.

Glucose biosensor based on open-source wireless microfluidic potentiostat

Conan Mercer[a,*], **Richard Bennett**[a], **Peter Ó. Conghaile**[b], **James F. Rusling**[a,c,d,e], **Dónal Leech**[a]

[a]School of Chemistry and Ryan Institute, National University of Ireland Galway, University Road, Galway, Ireland [b]National Centre for Sensor Research, School of Chemical Sciences, Dublin City University, Dublin 9, Ireland [c]Department of Chemistry, University of Connecticut, Storrs, CT 06269-3060, United States [d]Institute of Materials Science, University of Connecticut, Storrs, CT 06269-3136, United States [e]Department of Surgery and Neag Cancer Centre, UConn Health, Farmington, CT 06030, United States

Abstract

Wireless potentiostats capable of cyclic voltammetry and amperometry that connect to the Internet are emerging as key attributes of future point-of-care devices. This work presents an "integrated microfluidic electrochemical detector" (iMED) three-electrode multi-potentiostat designed around operational amplifiers connected to a powerful WiFi-based microcontroller as a promising alternative to more expensive and complex strategies reported in the literature. The iMED is integrated with a microfluidic system developed to be controlled by the same microcontroller. The iMED is programmed wirelessly over a standard WiFi network and all electrochemical data is uploaded to an open-source cloud-based server. A wired desktop computer is not necessary for operation or program uploading. This method of integrated microfluidic automation is simple, uses common and inexpensive materials, and is compatible with commercial sample injectors. An integrated biosensor platform contains four screen-printed carbon arrays inside 4 separate microfluidic detection chambers with Pt counter and pseudo Ag/AgCl reference electrodes in situ. The iMED is benchmarked with $K_3[Fe(CN)_6]$ against a commercial potentiostat and then as a glucose biosensor using glucose-oxidising films of [Os(2,2′-bipyridine)$_2$(polyvinylimidazole)$_{10}$Cl] prepared on screen-printed electrodes with multi walled carbon nanotubes, poly(ethylene glycol) diglycidyl ether and flavin adenine dinucleotide-dependent glucose dehydrogenase. Potential application of this cost-effective wireless potentiostat approach to modern bioelectronics and point-of-care diagnosis is demonstrated by production of glucose oxidation currents, under pseudo-physiological conditions, using mediating films with lower redox potentials.

*Corresponding author. c.mercer1@nuigalway.ie (C. Mercer).

Appendix A. Supplementary data

Supplementary data associated with this article can be found, in the online version, at https://doi.org/10.1016/j.snb.2019.02.031.

Keywords

Wireless; Open-source; Enzyme-based biosensor; Microfluidic biosensor; Smartphone; IoT

1. Introduction

Some of the most important challenges in point-of-care biosensor research are miniaturization, wireless data transmission and fully functional integrated devices [1,2]. Electrochemical biosensors explore measurements of an electrical signal produced on an electrochemical transducer applicable to addressing these challenges. A potentiostat is the electronic hardware required to control and run most electro-analytical experiments. The literature reports on many cost-effective open-source potentiostat platforms [3–10], however none integrate both microfluidics and wireless technology.

Designing systems with microfluidics rather than conventional laboratory analysis procedures can lead to miniaturization, increased throughput and reduced reagent consumption [11]. However, most existing fluid flow techniques rely on manual or semi-automated hardware. To combat this, programmed control over microfluidics is one target towards highly integrated, point-of-care clinical diagnostic devices for home and hospital use [12–17]. To this end, potentiostatic microfluidic biosensors must include some sort of standalone programmable controller for data acquisition, precise flow rate control and direction.

Automation in microfluidics has been applied to the extraction of nucleic acids [18], rotating disc based analysis of infectious diseases [19], flow cytometry [20], magnetic stirring [21], genetic stability with multiplexed PCR [22], chemiluminescence detection [23] and protein immunoblotting [24]. This research has brought about the search for a new generation of improved flow control and automation that satisfy requirements such as cost-effectiveness, all-in-one instrumentation and other complexity [25].

Recent efforts to automate liquid flow and direction include a report [26] on a bluetooth enabled microfluidic liquid handling system that utilised a microcontroller, solenoid valves and pneumatic pressure. The system capability was demonstrated by application to a bead-based HIV1 p24 sandwich immunoassay on a multi-layer poly-dimethylsiloxane (PDMS) chip. The Rusling group [27] demonstrated an automated electrochemiluminescence based system that combined a microcontroller, commercial micropumps and a charge coupled device camera for detection of proteins related to prostate cancer. Tan et al. [28] presented a platform for controlled fluid flow, where driving force is supplied by compressed nitrogen, via desktop computer for a multiplexed photonic crystal enhanced fluorescence detection of protein biomarkers interleukin 3 and Tumor Necrosis Factor α. Innovation in microfluidic directional control has seen introduction of valves that are torque-actuated [29,30], magnetic [29,31,32], solenoid [26,33–37] and pressure driven [14,38]. We integrate into the microfluidic platform for the first time, to our knowledge, independently controlled, electrically actuated servo-valves. The servo-valves are inexpensive relative to off-the-shelf commercially available automated microfluidic valve control options [13].

Here we integrate automated microfluidic flow and direction with the iMED, a wireless multi-potentiostat platform using inexpensive mass-produced components: the ESP-32 microcontroller, operational amplifiers (op-amps), high torque electromechanical servo-valves, and commercial syringe pump. Microcontroller incorporation allows for a generic and consistent route towards miniaturization, integration, automation and wireless connectivity of electrochemical protocols, identified as goals within the literature [39,40].

The iMED implements custom protocols, sequencing events and electrochemical analysis in a rapid and simple manner using the high-level programming language C/C++ with the open-source Arduino programming software. The ESP-32 microcontroller is approved by the FCC and CE regulatory requirements necessary for manufacture and sale in the United States and European Economic Area which could increase enthusiasm for the introduction of this technology to the market [13].

The entire iMED platform is designed to operate without a desktop computer. To this end, the iMED uses over the air updates (OTA) mechanism which allows the potentiostat to update itself based on data received while the normal firmware is running (for example, over WiFi). The device also sends all electrochemical data to an open-source cloud-based server for data post-processing [41]. This data is then visualised and accessible via any Internet connected device, such as a smart phone, tablet, laptop or wearable. The assembled wireless potentiostat requires only rudimentary instruction to use and here we demonstration the use of the iMED using an electrochemical enzyme-amplified biosensor to achieve detection of glucose concentrations in solution. Glucose sensing is critical to diagnosis, monitoring and treatment of the currently incurable diabetes disease [42].

Advancements in the application of enzymatic electrodes towards biosensors and bio-powered devices have been made in recent decades. Enzymes are an attractive route towards biocatalysis due to their inherent substrate specificity and ability to operate under mild conditions [43–45]. One such application of this is with immobilisation of glucose oxidising enzymes at an electrode surface. While glucose oxidase (GOx) is the most reported enzyme for this application, Flavin adenine dinucleotide-dependent glucose dehydrogenase (FADGDH) is more suitable than GOx due to its lack of reactivity with molecular oxygen. Previous work reported by us has demonstrated the improved suitability of FADGDH over GOx for such applications [46,47]. The combination of redox polymer films with enzymes on electrode surfaces to mediate electron transfer between active site and electrode surface has been widely demonstrated. Osmium based redox polymers consisting of an osmium centre attached to polymers such as poly(N-vinylimidazole) have been reported [48–54]. The suitability of osmium based redox centres is due to their relative stability, tunable redox potential and ability to operate at low potentials [55,56]. More recently, the addition of nano-supports such as multi-walled carbon nanotubes (MWCNTs) to the biofilm has resulted in increased current response as well as improved stability of the biofilms [57–61]. The use of crosslinkers such as glutaraldehyde or poly(ethylene glycol) diglycidyl ether (PEGDGE) to increase biofilm stability has been investigated previously [62,63]. Here we report on biofilms containing the redox polymer $[Os(2,2'\text{-bipyridine})_2(\text{poly-vinylimidazole})_{10}Cl]^+$ (Os(bpy)PVI) with the glucose oxidising enzyme FADGDH and MWCNTs crosslinked

using PEGDGE immobilised on screen printed carbon electrodes for the detection of glucose using the iMED potentiostatic microfluidic platform.

2. Experimental

2.1. Materials

PDMS, Sylgard 184 was purchased from Sigma and used with a ratio of 1:10 PDMS per master mold. Sodium phosphate dibasic, sodium phosphate monobasic monohydrate, sodium chloride, potassium chloride, was purchased from Sigma. All solutions were prepared using deionized water. Rheodyne 7725i injector was purchased from Sigma and used as received. Screen-printed carbon arrays consisting of eight 850 micrometer diameter sensors were from Kanichi Research (UK). 4-Port Switching Valves were from Upchurch Scientific. The component cost of the potentiostat is below 30 USD. In this calculation, the equipment costs (syringe pump and microfluidic components) were not included. The full list of electronic parts are available in Section 4.4 of the Supporting Information.

The flavin dependent glucose dehydrogenase is from Aspergillus sp. (FADGDH 1.1.99.10, Sekisui, Cambridge, USA; product GLDE-70–1192). The MWCNTs (product 659258; Sigma-Aldrich) were pretreated under reflux in concentrated nitric acid for 6 h and isolated by filtration. Polyethylene glycol diglycidyl ether (PEGDGE) was purchased from Sigma-Aldrich (average Mn 526). All aqueous solutions unless otherwise stated were prepared in Milli-Q water (1818 MΩ cm). The [Os(2,2′-bipyridine)2(polyvinylimidazole)$_{10}$Cl]+ (Os(bpy)PVI) redox polymer were synthesised according to literature procedures [64,65]. Characterization of (Os(bpy)PVI) is available in Section 2 of the Supporting Information.

The artificial plasma contained uric acid (68.5 mg l^{-1}), ascorbic acid (9.5 mg l^{-1}), fructose (36 mg l^{-1}), lactose (5.5 mg l^{-1}), urea (267 mg l^{-1}), cysteine (18 mg l^{-1}), sodium chloride (6.75 g l^{-1}), sodium bicarbonate (2.138 g l^{-1}), calcium sulfate (23.8 mg l^{-1}), magnesium sulfate (104.5 mg l^{-1}) and bovine serum albumin (7 g l^{-1}).

2.2. Hardware design

The electronic design that forms the basis of the iMED is described in two parts: the digital and the analogue designs. In addition the power supply and microfluidic designs are discussed. Firstly the power supply is described because it is continually referenced in all subsequent subsections. Secondly the digital design includes the ESP-32 microcontroller for waveform generation and data acquisition, dual-core processing and WiFi upload to a cloud-based server and an analog-to-digital converter (ADC) because its output is digital. Thirdly, the analogue design includes an electronic circuit based around op-amps, and a digital-to-analog converter (DAC) because its output is analogue. Finally microfluidic design which discusses electromechanical servo-valves, syringe pumping and electrochemical detection chambers. Also present in this section is a program that was developed in MATLAB that post-processes data uploaded to a cloud based server that plots amperometry data. Detailed circuit schematics are available as Supporting Information Section 4. All electronic components are mounted on a solderless breadboard, commonly used for prototyping due to their speed and ease when adding or changing components [33,66–68], printed circuit

boards can also be used and provide a more permanent solution [69], even though more difficult to rearrange components in the proof of concept phase.

2.3. Power supply

The iMED is designed to be a completely integrated instrument, only requiring electrode connectors and a power supply. The iMED does not require a desktop PC or laptop to operate. A power supply is necessary to supply the correct voltage and current to each active component in the circuit. A reconfigured L305P-01 desktop ATX power supply (Dell) is used to reduce the overall cost of the design. The power supply can deliver 3.3, 5, −12 and 12 V. The 5 V rail supplies the ESP-32 via the 5 V in pin. The ADC/DAC, not introduced yet but are external to the ESP-32, require additional power supply in order to guarantee a stable voltage reference. In both cases this power is provided by the stable 5 V rail of the ATX power supply.

As for the current reading part of the design, the ADS1115 ADC operating in single ended mode (measuring the voltage between the analog input channel and analog ground) requires a bias potential of −5 V in order to offset the current reading so the maximum values of current, positive and negative, are in the range 0–5 V. This bias potential is achieved using the LM79L05 negative regulator with a 0.1 μF output capacitor that provides a stable −5 V from the −12 V rail of the ATX power supply.

The circuit uses LM324 op-amps that require a symmetrical power supply. The LM79L08 and LM78L08 negative and positive regulators are used for bipolar (−8 and 8 V) supply to the op-amps.

2.4. Digital design

The ESP-32 is a Xtensa dual-core 32-bit microprocessor, 160 MHz, 600 DMIPS, WiFi: 802.11 b/g/n, Bluetooth Low Energy (BLE), that is used as the central processing unit for the potentiostat.

We use the WiFi capability instead of the BLE because of relatively higher bandwidth, larger coverage area, and increased cost-effectiveness due to WiFi network prevalence in buildings and cities compared to BLE [70,40]. To our knowledge, the literature reports on one previously published open-source wireless potentiostat using BLE [10], which confines wireless data transfer to a mobile phone. WiFi allows connection to any internet connected device and facilitates OTA, making it a more versatile device.

The ESP-32 is wirelessly programmed via WiFi using OTA updates, previously published potentiostats, both wired [3–9] and wireless [10], required a wired connection to the microcontroller to upload necessary computer programs, diminishing point-of-care applications. Once the ESP-32 is wirelessly programmed (details as Supporting Information, Section 5.5), a smart phone is used to connect to the ESP-32, which is then used to type WiFi credentials and set potential to be applied when in amperometry mode (detailed smart phone connectivity is available as Supporting Information, Section 5.4). In order to improve performance and versatility, both processor cores are programmed with ESP-IDF FreeRTOS (real-time operating system) embedded into the Arduino IDE core. This real-time operating

system allows the ESP-32 to run tasks in both CPU cores. This dual core technology is used with one core dedicated to the DAC and the other to the ADC. It is worth noting that if only one core is used, accurate scan rates > 100 mV s^{-1} cannot be obtained because the time taken to read the ADC input exceeds the time needed to apply the potential via the DAC.

The op-amp in a summing amplifier configuration is used to apply a potential window output between negative and positive values controlled by the DAC input. The design of the summing amplifier is a compromise between the potential resolution and potential window width. The ESP-32 has a reported built in two channel 8-bit digital-to-analog converter (DAC) [71]. Instead, for digital-to-analog conversion, important when applying a programmable potential via the potentiostat, we use an external MCP4725 DAC ([72]). The key attributes of the MCP4725 DAC are; 12-bit resolution, fast settling time (0.6 μs) which is the time required for the output to reach and remain within a given error band following the ESP-32 input stimulus, single-supply operation: 2.7–5.5 V, and I^2C communication. The external MCP4725 12-bit DAC is used to provide a resolution an order of magnitude over the ESP-32 internal lower resolution 8-bit DAC, and therefore greater precision within the 2 V potential window. The MCP4725 DAC provides 2^{12} = 4096 quantization levels with a sensitivity of 5 V/4096 = 1.2 mV in the voltage output range. The DAC is powered by 5 V to create a 5 V potential for the summing amplifier circuit configuration. This 5 V potential overcomes the 3.3 V ESP-32 built in logic that would otherwise limit the potential window applied to the op-amp circuit for the potentiostat. The DAC requires a 5 V reference voltage, which must be stable, that is supplied via the reconfigured ATX power supply. For cost-effective comparisons of various DACs used within the literature, see Supporting Information, Section 4.2.1.

2.5. Analogue design

Electrical signals between the three electrode electrochemical cell and the ESP-32 is based on a circuit implemented with the op-amp in a transimpedance amplifier (TIA) configuration. TIA configuration is used to convert the signal current from working electrode (WE) into a voltage. This voltage is read by the external 16-bit ADC [66], that provides greater quantization levels over the internal 12-bit ADC on the ESP-32 and many custom built potentiostats in the literature [5,73,74], it provides equal quantization to one report by Cruz et al. [6], however not as powerful as one report by Dryden et al. [8] compromise being cost. The 16-bit ADC uses a signed integer [75]; therefore 2^{15} = 32, 768 quantization levels with a sensitivity of 5 V/32768 = 0.15 mV in the voltage input range. The TIA circuit is duplicated allowing four channels whose timing is synchronized by the programmed ESP-32. The wireless potentiostat part of the iMED is 8 × 11 × 1.85 cm in dimensions, which is significantly smaller than the commercial CHI 1030 (36 × 24 × 12 cm) used to benchmark the iMED. This represents a significant percentage difference in volume cm^3 (193%) in support of the iMED.

2.6. Microfluidic design

The ESP-32 controlled microfluidic platform configuration consists of one syringe pump (Aladdin AL-1000), three assembled servo-valves and four detection chambers (Fig. 1). Each electromechanical servo-valve is connected to the microcontroller directly using

general-purpose input/output (GPIO) pins and powered by the 5 V rail of the ATX power supply. The ESP-32 is a versatile, low cost, standalone WiFI based microcontrolled platform with a small footprint (55 × 28 × 12 mm). This size makes it suitable for controlling many different types of microfluidic platforms. Alternatives to the ESP-32 include, Arduino, Teensy, Raspberry Pi and BeagleBone microcontrollers/processors that have been used in analytical chemistry platforms [33,34,36,67,68,76–81], although most do not have any kind of wireless connectivity, and the latter two are not cost-effective. For cost-effective comparisons of various microcontrollers used within the literature, see Supporting Information, Section 1.2. The syringe pump uses serial communication. Therefore, the syringe pump is connected to the ESP-32 via a MAX232 integrated circuit that converts signals from the syringe pump RS-232 serial port to signals suitable for use in TTL-compatible ESP-32 (Section 1.5 of the Supporting Information). The ESP-32 sends serial commands to the syringe pump at a default baud rate of 19200 bps, although the syringe pump can be programmed to different rates if required. The main function of the microfluidic part of the C/C++ program is to actuate the servo-valves at defined times and initiate the syringe pump at specified flow rates.

2.6.1. Electromechanical servos—Servos are secured to valves using medical grade epoxy glue, each servo-valve can rotate 180° and has two flow path options (Fig. 2). Each actuator is controlled by the C/C++ program uploaded to the iMED. In order to change direction of fluid, a square wave of 5 V amplitude is applied to the actuator using the program-controlled ESP-32 (Section 1.3 of the Supporting Information). The first actuated valve in the sequence directs flow to either detection chambers 1 and 2 or 3 and 4, while the second and third actuated valve controls flow into 1–4 detection streams (Fig. 1). Each servo-valve has a reported low swept-volume, can withstand pressures up-to 500 psi (34 bar), is chemically inert and biocompatible [82]. Actuation is reported to occur over a short period of 150 ms through 60° at an applied potential of 6 V, or 190 ms through 60° at an applied potential of 4.8 V [83]. Actuation speed is therefore sufficiently fast enough for microfluidic direction change.

2.7. Electrochemical measurements

Placement for the working electrode (WE), counter electrode (CE) and reference electrode (RE) is inside a PDMS slab (created using a machined mold) with a 1.5 mm wide rectangular channel, creating four 63 μl electrochemical detection chambers previously reported [84]. The WE is a Kanichi array with a format of 8 carbon screen printed electrodes (dia. 850 μm). Kanichi electrode arrays have been used previously in biosensor research [84–86]. Each of the four Kanichi arrays used are short circuited to provide one WE for each channel of the potentiostat. All samples are injected manually into the microfluidic system using a 100 μl loop and Rheodyne 7725i sample injector, except Section 3.1.2 where a traditional beaker electrochemical cell is used.

Enzyme electrode assembly is achieved by depositing appropriate volumes from 5 mg ml^{-1} redox polymer aqueous solution, 10 mg ml^{-1} FADGDH aqueous solution, 46 mg ml^{-1} aqueous dispersion of acid-treated MWCNTs and 15 mg ml^{-1} PEGDGE aqueous solution on the surface of the Kanichi working electrode and allowing the deposition to dry for 24 h.

3. Results and discussion

3.1. System testing and validation

3.1.1. Resistor polarization—Ohms law states there is a linear relationship between voltage and current. Resistors are ohmic materials that are useful in the analysis of electrical circuits. Ohm's law is satisfied when the voltage vs current plot for a resistor of known value is a straight line through the origin. This known response is tested with various resistors and is plotted using data acquired from a commercial CHI 1030 (CH Instruments) potentiostat and the iMED: $R^2 = 0.999$ for 5.1 kΩ, 7.1 kΩ, and 10 kΩ, Fig. 3. These results compare well to other reports in the literature [5,73,74], and suggest a strong positive linear relationship between the iMED and the CHI 1030 in the microamp scale throughout the 2 V ± 200 μA operation range.

3.1.2. Cyclic voltammetry—Once the resistor polarization curve verified the iMED circuit was working as expected, the device was tested to validate its functionality. It was observed that the device effectively performed full range CV measurements on three-electrode set-ups in the voltage range between 1 and −1 V. The data obtained is stored in the internal memory of the microcontroller. Using both CPU cores, the C/C++ program is designed in such a way that voltage and current data is stored locally and then exported via WiFI upload to a ThingSpeak (MathWorks) web server to be stored as a comma separated values text file.

For validation, cyclic voltammetry (CV) studies of platinum working electrode with a diameter of 1.6 mm were performed in potassium chloride (0.1 M) containing 19.35 mM potassium ferricyanide using the CHI 1030 and the iMED. Potassium ferricyanide in this concentration range is consistently reported in the literature to validate potentiostats of this type [6,5,10].

The four channels of the iMED were also compared. Each channel is subjected to the same parameters with the scan rate (100 mV s^{-1}) and the detection limits ($-0.2 \leq V_{we-re} \leq 0.8$) for both experiments. The resulting plots were compared, and it was found that both CV curves exhibit well-defined oxidation and reduction peaks of the redox moieties with identical magnitude of current response (1% variation in magnitude of current response) Fig. 4. Redox potentials are also compared to the CHI 1030 and show a 1.25% variance in redox potentials, 0.219 V and 0.222 V, iMED and CHI 1030 respectively, Fig. 5.

3.1.3. Amperometry—Reproducibility within a single electrochemical detection chamber was tested using $K_3[Fe(CN)_6]$ by running amperometry (reduction current) and injecting various concentrations of $K_3[Fe(CN)_6]$ (2.5–15mM) in triplicate. The percentage relative standard deviation of the measurements for the 4 concentrations is, 3.66, 2.21, 0.89, 1.39 (% RSD), respectively. The equation of the line and correlation coefficient is $y = 1.26162x + -1.9174$ $R^2 = 0.98$ and the standard deviation is indicated by error bars, (Fig. 6), confirming good peak-to-peak reproducibility of the potentiostat operating in amperometry mode. This data is in strong agreement with data from a similar experiment used to validate an open-source potentiostat [74]. The Supporting Information, Section 5.9 provides the

source code for performing MATLAB graphical visualization of amperometric data to be viewed on an internet connected smartphone.

3.1.4. Microcontrolled syringe pump and programmed control of flow rates—

Automation of syringe pumps eliminates manual operational pump control and can achieve complete governance over flow rates and times in programmed biosensor experiments. While computer software is available to control syringe pumps at a cost [87,88], desktop computer connections diminish point of care applications. We report here, for the first time to our knowledge, microcontrol of a common Aladdin AL-1000 syringe pump using the ESP-32 microcontroller. To this end, the syringe pump is connected to the microcontroller via a MAX232 chip (see Section 2.6). The MAX232 is necessary to convert TIA-232 (RS-232) syringe pump serial port to signals suitable for use with the TTL-compatible digital logic circuits on the ESP-32, see Section 2.6. To test the hardware connection a terminal emulator program (RealTerm, on Microsoft Windows) is setup with RS-232 protocol (Section 1.5 of the Supporting Information) and used to communicate with the pump in hexadecimal commands via a PC. The command 'VER' is sent to which the pump responds with its model and firmware version. The benefit of initially using a terminal emulator to gain response from the pump is to verify that the hardware is working correctly. Syringe pump syntax is investigated using this terminal emulator concept. Development of the pumping sequence (Section 1.6 of the Supporting Information) is then coded onto the microcontroller. The pump and microcontroller maintain stable communication throughout 100 repetitions of a test pump flushing program, using water as a test medium. This programmed microcontrolled pump is capable of a reported flow rate range between 0.01 μL min^{-1} and 28.3 mL min^{-1}, and can be expanded to achieve simultaneous control of multiple pumps connected in a network if required [89]. Back flow within microfluidic systems can cause possible reagent contamination [90], and because servo-valves can withstand pressures of 500 psi, any resulting back pressure due to excessive force needed to drive the syringe could stall the pump. To avoid this back pressure the microcontroller is not programmed to simultaneously close servo-valves and cease pumping at 2000 μL min^{-1} flow rates. Instead, by applying a square wave at 5 V for a defined time period, servo-valves close 10 s after terminating pump flow. By alternating square waves in this defined time sequence, back pressure opposed to the desired flow path that would otherwise result in a pump stall is avoided. Also, the fluid source, pump, and fluid outlet are maintained at the same height to minimize back pressure [91]. Connection to the microfluidic detection chambers is achieved using conventional 0.2 mm i.d. PEEK tubing.

3.2. Amperometric glucose biosensor

For detection of glucose in solution, glucose concentrations were loaded into the sample loop, and injected into the detection chamber. Glucose oxidising currents were recorded by the iMED (Fig. 7) and the peak area currents increased linearly with physiologically relevant concentrations of 1 to 10 mM glucose (Fig. 8). Reproducibility was tested for glucose concentrations by running the experiment on different working electrodes with different Kanichi arrays. Standard deviation of the measurements for the 10 concentrations, indicated by error bars, confirmed good array-to-array and electrode-to-electrode reproducibility (Fig. 8).

Slow scan cyclic voltammograms in artificial plasma in the presence of glucose for films of co-immobilised with Os(bpy)PVI, PEGDGE, MWCNTs and FADGDH on Kanichi array electrodes show sigmoidal shaped curves, providing steady-state glucose oxidation currents above potentials for the Os(II/III) redox transition, indicative of EC' electrocatalysis of glucose, see Supporting Information, Section 3.

The redox potential of [Os(2,2′-bipyridine)$_2$(poly-vinylimidazole)$_{10}$Cl] is ~0.22 V [56]. Because the iMED works in the −1 V to 1 V ± 200 μA range, the device is suitable for detection of glucose oxidation currents using this electron mediator.

4. Conclusions

In this work, we designed, fabricated, and demonstrated a new wireless multi-potentiostat biosensor (iMED) performing integrated microfluidic electrochemical glucose detection. The main technical limitation, the potential window of the iMED compared to commercial potentiostat operational window (−1 V to 1 V), is overcome through the use of a tailored redox polymer, Os(bpy)PVI, within the potential range of the iMED. To assess the iMED performance, the system was compared with a commercial potentiostat commonly used in electrochemical research using $K_3[Fe(CN)_6]$, with strong agreement between data obtained. Electrochemical cyclic voltammetry and amperometry is delivered in a simple, inexpensive, ambient lab environment that interfaces with a wirelessly programmed microcontroller that uploads all data to an open-source cloud-based server. The interface is comprised of a syringe pump and servo actuated valves that automate the flushing, washing and detection of glucose in solution. This control in microfluidic technology is applicable beyond glucose detection [11]. The system is sealed with conventional PEEK tubing and leak free flangeless fittings. This open-source approach could be implemented and adapted into modern bioelectrochemical laboratories in a variety of microfluidic experiments in a cost-effective, powerful, and wireless manner. Future works could focus on other biosensors based on similar enzyme-based designs that would utilise the multiple working electrodes, for example, multiplexed biomarker biosensors.

Supplementary Material

Refer to Web version on PubMed Central for supplementary material.

Acknowledgement

This work was supported financially by Science Foundation Ireland under the US/Ireland programme (Grant Number 13/US/B2546).

References

[1]. Kim J, Campbell AS, Wang J, Wearable non-invasive epidermal glucose sensors: a review, Talanta 177 (2018) 163–170, 10.1016/j.talanta.2017.08.077. [PubMed: 29108571]

[2]. Pruna R, Palacio F, Baraket A, Zine N, Streklas A, Bausells J, Errachid A, López M, A low-cost and miniaturized potentiostat for sensing of biomolecular species such as TNF-α by electrochemical impedance spectroscopy, Biosens. Bioelectron 100 (2018) 533–540, 10.1016/j.bios.2017.09.049. [PubMed: 28988118]

[3]. Beach R, Conlan R, Godwin M, Moussy F, Towards a miniature implantable in vivo telemetry monitoring system dynamically configurable as a potentiostat or galvanostat for two- and three-electrode biosensors, IEEE Trans. Instrum. Meas 54 (2005) 61–72, 10.1109/TIM.2004.839757.

[4]. Huang CY, Syu MJ, Chang YS, Chang CH, Chou TC, Liu BD, A portable potentiostat for the bilirubin-specific sensor prepared from molecular imprinting, Biosens. Bioelectron 22 (2007) 1694–1699, 10.1016/j.bios.2006.07.036. [PubMed: 16962762]

[5]. Meloni GN, Building a microcontroller based potentiostat: a inexpensive and versatile platform for teaching electrochemistry and instrumentation, J. Chem. Educ 93 (2016) 1320–1322, 10.1021/acs.jchemed.5b00961.

[6]. Cruz AFD, Norena N, Kaushik A, Bhansali S, A low-cost miniaturized potentiostat for point-of-care diagnosis, Biosens. Bioelectron 62 (2014) 249–254, 10.1016/j.bios.2014.06.053. [PubMed: 25016332]

[7]. Rowe A.a., Bonham AJ, White RJ, Zimmer MP, Yadgar RJ, Hobza TM, Honea JW, Ben-Yaacov I, Plaxco KW, CheapStat: an open-source, “do-it-your-self” potentiostat for analytical and educational applications, PLoS ONE 6 (2011) e23783, 10.1371/journal.pone.0023783. [PubMed: 21931613]

[8]. Dryden MDM, Wheeler AR, DStat: a versatile, open-source potentiostat for electroanalysis and integration, PLOS ONE 10 (2015) e0140349, 10.1371/journal.pone.0140349. [PubMed: 26510100]

[9]. Kwakye S, Baeumner A, An embedded system for portable electrochemical detection, Sens. Actuators B Chem 123 (2007) 336–343, 10.1016/j.snb.2006.08.032.

[10]. Ainla A, Mousavi MPS, Tsaloglou MN, Redston J, Bell JG, Fernández-Abedul MT, Whitesides GM, Open-source potentiostat for wireless electrochemical detection with smartphones, Anal. Chem 90 (2018) 6240–6246, 10.1021/acs.analchem.8b00850. [PubMed: 29658268]

[11]. Mercer C, Jones A, Rusling JF, Leech D, Multiplexed electrochemical cancer diagnostics with automated microfluidics, Electroanalysis (2018) 1–5, 10.1002/elan.201800632.

[12]. Whitesides GM, The origins and the future of microfluidics, Nature 442 (2006) 368–373, 10.1038/nature05058. [PubMed: 16871203]

[13]. Volpatti LR, Yetisen AK, Commercialization of microfluidic devices, Trends Biotechnol 32 (2014) 347–350, 10.1016/j.tibtech.2014.04.010. [PubMed: 24954000]

[14]. Au AK, Bhattacharjee N, Horowitz LF, Chang TC, Folch A, 3D-printed microfluidic automation, Lab Chip 15 (2015) 1934–1941, 10.1039/C5LC00126A. [PubMed: 25738695]

[15]. Mark D, Haeberle S, Roth G, von Stetten F, Zengerle R, Microfluidic lab-on-a-chip platforms: requirements, characteristics and applications, Chem. Soc. Rev 39 (2010) 1153, 10.1039/b820557b. [PubMed: 20179830]

[16]. Rusling JF, Multiplexed electrochemical protein detection and translation to personalized cancer diagnostics, Anal. Chem 85 (2013) 5304–5310, 10.1021/ac401058v. [PubMed: 23635325]

[17]. Xu D, Huang X, Guo J, Ma X, Automatic smartphone-based microfluidic biosensor system at the point of care, Biosens. Bioelectron 110 (2018) 78–88, 10.1016/j.bios.2018.03.018. [PubMed: 29602034]

[18]. Wen J, Legendre LA, Bienvenue JM, Landers JP, Purification of nucleic acids in microfluidic devices, Anal. Chem 80 (2008) 6472–6479, 10.1021/ac8014998. [PubMed: 18754652]

[19]. Lee BS, Lee JN, Park JM, Lee JG, Kim S, Cho YK, Ko C, A fully automated immunoassay from whole blood on a disc, Lab Chip 9 (2009) 1548, 10.1039/b820321k. [PubMed: 19458861]

[20]. Maecker HT, McCoy JP, Nussenblatt R, Standardizing immunophenotyping for the Human Immunology Project, Nat. Rev. Immunol 12 (2012) 191–200, 10.1038/nri3158. [PubMed: 22343568]

[21]. Mercer C, Leech D, Inexpensive miniature programmable magnetic stirrer from reconfigured computer parts, J. Chem. Educ 94 (2017) 816–818, 10.1021/acs.jchemed.7b00184.

[22]. Chen Y, Zhang B, Feng H, Shu W, Chen GY, Zhong JF, An automated microfluidic device for assessment of mammalian cell genetic stability, Lab Chip 12 (2012) 3930, 10.1039/c2lc40437k. [PubMed: 22814625]

[23]. Tang CK, Vaze A, Rusling JF, Automated 3D-printed unibody immunoarray for chemiluminescence detection of cancer biomarker proteins, Lab Chip 17 (2017) 484–489, 10.1039/C6LC01238H. [PubMed: 28067370]

[24]. He M, Herr AE, Automated microfluidic protein immunoblotting, Nat. Protoc 5 (2010) 1844–1856, 10.1038/nprot.2010.142. [PubMed: 21030959]

[25]. Sackmann EK, Fulton AL, Beebe DJ, The present and future role of microfluidics in biomedical research, Nature 507 (2014) 181–189, 10.1038/nature13118. [PubMed: 24622198]

[26]. Li B, Li L, Guan A, Dong Q, Ruan K, Hu R, Li Z, A smartphone controlled handheld microfluidic liquid handling system, Lab Chip 14 (2014) 4085–4092, 10.1039/C4LC00227J. [PubMed: 25182078]

[27]. Kadimisetty K, Malla S, Sardesai NP, Joshi AA, Faria RC, Lee NH, Rusling JF, Automated multiplexed ECL immunoarrays for cancer biomarker proteins, Anal. Chem 87 (2015) 4472–4478, 10.1021/acs.analchem.5b00421. [PubMed: 25821929]

[28]. Tan Y, Tang T, Xu H, Zhu C, Cunningham BT, High sensitivity automated multiplexed immunoassays using photonic crystal enhanced fluorescence microfluidic system, Biosens. Bioelectron 73 (2015) 32–40, 10.1016/j.bios.2015.05.041. [PubMed: 26043313]

[29]. Weibel DB, Kruithof M, Potenta S, Sia SK, Lee A, Whitesides GM, Torque-actuated valves for microfluidics, Anal. Chem 77 (2005) 4726–4733, 10.1021/ac048303p. [PubMed: 16053282]

[30]. Elizabeth Hulme S, Shevkoplyas SS, Whitesides GM, Incorporation of pre-fabricated screw, pneumatic, and solenoid valves into microfluidic devices, Lab Chip 9 (2009) 79–86, 10.1039/B809673B. [PubMed: 19209338]

[31]. Chen CY, Chen CH, Tu TY, Lin CM, Wo AM, Electrical isolation and characteristics of permanent magnet-actuated valves for PDMS microfluidics, Lab Chip 11 (2011) 733–737, 10.1039/C0LC00415D. [PubMed: 21132206]

[32]. Cao Q, Han X, Li L, Configurations and control of magnetic fields for manipulating magnetic particles in microfluidic applications: magnet systems and manipulation mechanisms, Lab Chip 14 (2014) 2762, 10.1039/c4lc00367e. [PubMed: 24903572]

[33]. Ting H, Hu JB, Hsieh KT, Urban PL, A pinch-valve interface for automated sampling and monitoring of dynamic processes by gas chromatography-mass spectrometry, Anal. Methods 6 (2014) 4652, 10.1039/c4ay00637b.

[34]. da Costa ET, Mora MF, Willis PA, do Lago CL, Jiao H, Garcia CD, Getting started with open-hardware: development and control of microfluidic devices, Electrophoresis 35 (2014) 2370–2377, 10.1002/elps.201400128. [PubMed: 24823494]

[35]. Wang KIK, Salcic Z, Yeh J, Akagi J, Zhu F, Hall CJ, Crosier KE, Crosier PS, Wlodkowic D, Toward embedded laboratory automation for smart lab-on-a-chip embryo arrays, Biosens. Bioelectron 48 (2013) 188–196, 10.1016/j.bios.2013.04.033. [PubMed: 23685315]

[36]. Cao Z, Chen F, Bao N, He H, Xu P, Jana S, Jung S, Lian H, Lu C, Droplet sorting based on the number of encapsulated particles using a solenoid valve, Lab Chip 13 (2013) 171–178, 10.1039/C2LC40950J. [PubMed: 23160342]

[37]. Riahi R, Shaegh SAM, Ghaderi M, Zhang YS, Shin SR, Aleman J, Massa S, Kim D, Dokmeci MR, Khademhosseini A, Automated microfluidic platform of bead-based electrochemical immunosensor integrated with bioreactor for continual monitoring of cell secreted biomarkers, Sci. Rep 6 (2016) 24598, 10.1038/srep24598. [PubMed: 27098564]

[38]. Ezra E, Maor I, Bavli D, Shalom I, Levy G, Prill S, Jaeger MS, Nahmias Y, Microprocessor-based integration of microfluidic control for the implementation of automated sensor monitoring and multithreaded optimization algorithms, Biomed. Microdevices 17 (2015) 82, 10.1007/s10544-015-9989-y. [PubMed: 26227212]

[39]. Patabadige DEW, Jia S, Sibbitts J, Sadeghi J, Sellens K, Culbertson CT, Micro total analysis systems: fundamental advances and applications, Anal. Chem 88 (2016) 320–338, 10.1021/acs.analchem.5b04310. [PubMed: 26599485]

[40]. Kassal P, Steinberg MD, Steinberg IM, Wireless chemical sensors and biosensors: a review, Sens. Actuators B Chem 266 (2018) 228–245, 10.1016/j.snb.2018.03.074.

[41]. Mercer C, Leech D, Cost-effective wireless microcontroller for internet connectivity of open-source chemical devices, J. Chem. Educ 95 (2018) 1221–1225, 10.1021/acs.jchemed.8b00200.

[42]. Bruen D, Delaney C, Florea L, Diamond D, Glucose sensing for diabetes monitoring: recent developments, Sensors 17 (2017) 1866, 10.3390/s17081866.

[43]. Calabrese Barton S, Gallaway J, Atanassov P, Enzymatic biofuel cells for implantable and microscale devices, Chem. Rev 104 (2004) 4867–4886, 10.1021/cr020719k. [PubMed: 15669171]

[44]. Leech D, Kavanagh P, Schuhmann W, Enzymatic fuel cells: recent progress, Electrochim. Acta 84 (2012) 223–234, 10.1016/j.electacta.2012.02.087.

[45]. Wang J, Carbon-nanotube based electrochemical biosensors: a review, Electroanalysis 17 (2005) 7–14, 10.1002/elan.200403113.

[46]. Bennett R, Osadebe I, Kumar R, Conghaile PÓ, Leech D, Design of experiments approach to provide enhanced glucose-oxidising enzyme electrode for membraneless enzymatic fuel cells operating in human physiological fluids, Electroanalysis (2018) 1–9, 10.1002/elan.201600402.

[47]. Osadebe I, Leech D, Effect of multi-walled carbon nanotubes on glucose oxidation by glucose oxidase or a flavin-dependent glucose dehydrogenase in redox-polymer-mediated enzymatic fuel cell anodes, ChemElectroChem 1 (2014) 1988–1993, 10.1002/celc.201402136.

[48]. Mao F, Mano N, Heller A, Long tethers binding redox centers to polymer back-bones enhance electron transport in enzyme “wiring” hydrogels, J. Am. Chem. Soc 125 (2003) 4951–4957, 10.1021/ja029510e. [PubMed: 12696915]

[49]. Chen T, Barton SC, Binyamin G, Gao Z, Zhang Y, Kim HH, Heller A, A miniature biofuel cell, J. Am. Chem. Soc 123 (2001) 8630–8631, 10.1021/ja0163164. [PubMed: 11525685]

[50]. Ohara TJ, Rajagopalan R, Heller A, Glucose electrodes based on cross-linked bis (2,2′-bipyridine)chloroosmium(+/2+) complexed poly(1-vinylimidazole) films, Anal. Chem 65 (1993) 3512–3517, 10.1021/ac00071a031. [PubMed: 8297033]

[51]. Mano N, Mao F, Heller A, Characteristics of a miniature compartment-less glucose-O2 biofuel cell and its operation in a living plant, J. Am. Chem. Soc 125 (2003) 6588–6594, 10.1021/ja0346328. [PubMed: 12785800]

[52]. Heller A, Electrical wiring of redox enzymes, Acc. Chem. Res 23 (1990) 128–134, 10.1021/ar00173a002.

[53]. Fedorov K, Blaszykowski C, Sheikh S, Reheman A, Romaschin A, Ni H, Thompson M, Prevention of thrombogenesis from whole human blood on plastic polymer by ultrathin monoethylene glycol silane adlayer, Langmuir 30 (2014) 3217–3222, 10.1021/la500745p. [PubMed: 24625256]

[54]. González-Guerrero MJ, del Campo FJ, Esquivel JP, Leech D, Sabaté N, Paper-based microfluidic biofuel cell operating under glucose concentrations within physiological range, Biosens. Bioelectron 90 (2017) 475–480, 10.1016/j.bios.2016.09.062. [PubMed: 27825524]

[55]. Ó Conghaile P, Pöller S, MacAodha D, Schuhmann W, Leech D, Coupling osmium complexes to epoxy-functionalised polymers to provide mediated enzyme electrodes for glucose oxidation, Biosens. Bioelectron 43 (2013) 30–37, 10.1016/j.bios.2012.11.036. [PubMed: 23274194]

[56]. Boland S, Kavanagh P, Leech D, Mediated enzyme electrodes for biological fuel cell and biosensor applications, ECS Trans. ECS (2008) 77–87, 10.1149/1.3036213.

[57]. Zebda A, Gondran C, Le Goff A, Holzinger M, Cinquin P, Cosnier S, Mediatorless high-power glucose biofuel cells based on compressed carbon nanotube-enzyme electrodes, Nat. Commun 2 (2011) 370, 10.1038/ncomms1365. [PubMed: 21712818]

[58]. Holzinger M, Le Goff A, Cosnier S, Nanomaterials for biosensing applications: a review, Front. Chem 2 (2014) 1–10, 10.3389/fchem.2014.00063.

[59]. Gao F, Viry L, Maugey M, Poulin P, Mano N, Engineering hybrid nanotube wires for high-power biofuel cells, Nat. Commun 1 (2010) 1–7, 10.1038/ncomms1000. [PubMed: 20975674]

[60]. MacAodha D, Ó Conghaile P, Egan B, Kavanagh P, Sygmund C, Ludwig R, Leech D, Comparison of glucose oxidation by crosslinked redox polymer enzyme electrodes containing carbon nanotubes and a range of glucose oxidising enzymes, Electroanalysis 25 (2013) 94–100, 10.1002/elan.201200536.

[61]. Ó Conghaile P, Falk M, MacAodha D, Yakovleva ME, Gonaus C, Peterbauer CK, Gorton L, Shleev S, Leech D, Fully enzymatic membraneless glucose|oxygen fuel cell that provides 0.275 mA cm^{-2} in 5 mM glucose, operates in human physiological solutions, and powers transmission

of sensing data, Anal. Chem 88 (2016) 2156–2163, 10.1021/acs.analchem.5b03745. [PubMed: 26750758]

[62]. MacAodha D, Ferrer ML, Conghaile PÓ, Kavanagh P, Leech D, Crosslinked redox polymer enzyme electrodes containing carbon nanotubes for high and stable glucose oxidation current, Phys. Chem. Chem. Phys 14 (2012) 14667, 10.1039/c2cp42089a. [PubMed: 23033161]

[63]. de Lumley-Woodyear T, Rocca P, Lindsay J, Dror Y, Freeman A, Heller A, Polyacrylamide-based redox polymer for connecting redox centers of enzymes to electrodes, Anal. Chem 67 (1995) 1332–1338, 10.1021/ac00104a006. [PubMed: 7741213]

[64]. Forster RJ, Vos JG, Synthesis, characterization, and properties of a series of osmium- and ruthenium-containing metallopolymers, Macromolecules 23 (1990) 4372–4377, 10.1021/ma00222a008.

[65]. Kober EM, Caspar JV, Sullivan BP, Meyer TJ, Synthetic routes to new polypyridyl complexes of osmium(II), Inorg. Chem 27 (1988) 4587–4598, 10.1021/ic00298a017.

[66]. Grinias JP, Whitfield JT, Guetschow ED, Kennedy RT, An inexpensive, open-source USB Arduino data acquisition device for chemical instrumentation, J. Chem. Educ 93 (2016) 1316–1319, 10.1021/acs.jchemed.6b00262. [PubMed: 27453587]

[67]. Chen CL, Chen TR, Chiu SH, Urban PL, Dual robotic arm “production line” mass spectrometry assay guided by multiple Arduino-type microcontrollers, Sens. Actuators B Chem 239 (2017) 608–616, 10.1016/j.snb.2016.08.031.

[68]. Meloni GN, 3D printed and microcontrolled: the one hundred dollars scanning electrochemical microscope, Anal. Chem (2017), 10.1021/acs.analchem.7b01764.

[69]. Jalal AH, Umasankar Y, Gonzalez PJ, Alfonso A, Bhansali S, Multimodal technique to eliminate humidity interference for specific detection of ethanol, Biosens. Bioelectron 87 (2017) 522–530, 10.1016/j.bios.2016.08.106. [PubMed: 27598854]

[70]. Li L, Xiaoguang H, Ke C, Ketai H, The applications of WiFi-based wireless sensor network in internet of things and smart grid, 2011 6th IEEE Conf. Ind. Electron. Appl. IEEE, 2011, pp. 789–793, 10.1109/ICIEA.2011.5975693.

[71]. Espressif, ESP32 Datasheet, (2018) https://www.espressif.com/sites/default/files/documentation/esp32_datasheet_en.pdf.

[72]. Haizad M, Ibrahim R, Adnan A, Chung TD, Hassan SM, Development of low-cost real-time data acquisition system for process automation and control, 2016 2nd IEEE Int. Symp. Robot. Manuf. Autom. IEEE, 2016, pp. 1–5, 10.1109/ROMA.2016.7847826.

[73]. Friedman ES, Rosenbaum MA, Lee AW, Lipson DA, Land BR, Angenent LT, A cost-effective and field-ready potentiostat that poises subsurface electrodes to monitor bacterial respiration, Biosens. Bioelectron 32 (2012) 309–313, 10.1016/j.bios.2011.12.013. [PubMed: 22209069]

[74]. Steinberg MD, Kassal P, Kereković I, Steinberg IM, A wireless potentiostat for mobile chemical sensing and biosensing, Talanta 143 (2015) 178–183, 10.1016/j.talanta.2015.05.028. [PubMed: 26078146]

[75]. Jin H, Qin Y, Pan S, Alam AU, Dong S, Ghosh R, Deen MJ, Open-source low-cost wireless potentiometric instrument for pH determination experiments, J. Chem. Educ 95 (2018) 326–330, 10.1021/acs.jchemed.7b00479.

[76]. D’Ausilio A, Arduino: A low-cost multipurpose lab equipment, Behav. Res. Methods 44 (2012) 305–313, 10.3758/s13428-011-0163-z. [PubMed: 22037977]

[77]. Wijnen B, Hunt EJ, Anzalone GC, Pearce JM, Open-source syringe pump library, PLOS ONE 9 (2014) e107216, 10.1371/journal.pone.0107216. [PubMed: 25229451]

[78]. Höfflin J, Torres Delgado SM, Suárez Sandoval F, Korvink JG, Mager D, Electrifying the disk: a modular rotating platform for wireless power and data transmission for Lab on a disk application, Lab Chip 15 (2015) 2584–2587, 10.1039/C5LC00138B. [PubMed: 25968976]

[79]. da Costa ET, Neves CA, Hotta GM, Vidal DTR, Barros MF, Ayon AA, Garcia CD, do Lago CL, Unmanned platform for long-range remote analysis of volatile compounds in air samples, Electrophoresis 33 (2012) 2650–2659, 10.1002/elps.201200273. [PubMed: 22965708]

[80]. Lillehoj PB, Huang MC, Truong N, Ho CM, Rapid electrochemical detection on a mobile phone, Lab Chip 13 (2013) 2950, 10.1039/c3lc50306b. [PubMed: 23689554]

[81]. Novo P, Chu V, Conde J, Integrated optical detection of autonomous capillary microfluidic immunoassays: a hand-held point-of-care prototype, Biosens. Bioelectron 57 (2014) 284–291, 10.1016/j.bios.2014.02.009. [PubMed: 24607579]

[82]. IDEX, 4-Way Valve PEEK Flow Valve, (2018) https://www.idex-hs.com/4-wayflow-valve-peek.html?optionvalue=6623.

[83]. TowerPro, MG996R High Torque Metal Gear Dual Ball Bearing Servo Datasheet, (2018) https://www.electronicoscaldas.com/datasheet/MG996R_Tower-Pro.pdf.

[84]. Chikkaveeraiah BV, Mani V, Patel V, Gutkind JS, Rusling JF, Microfluidic electrochemical immunoarray for ultrasensitive detection of two cancer biomarker proteins in serum, Biosens. Bioelectron 26 (2011) 4477–4483, 10.1016/j.bios.2011.05.005. [PubMed: 21632234]

[85]. Otieno BA, Krause CE, Latus A, Chikkaveeraiah BV, Faria RC, Rusling JF, Online protein capture on magnetic beads for ultrasensitive microfluidic immunoassays of cancer biomarkers, Biosens. Bioelectron 53 (2014) 268–274, 10.1016/j.bios.2013.09.054. [PubMed: 24144557]

[86]. Wasalathanthri DP, Faria RC, Malla S, Joshi AA, Schenkman JB, Rusling JF, Screening reactive metabolites bioactivated by multiple enzyme pathways using a multiplexed microfluidic system, Analyst 138 (2013) 171–178, 10.1039/C2AN35993F. [PubMed: 23095952]

[87]. Gaikwad AM, Gallaway JW, Desai D, Steingart DA, Electrochemical-mechanical analysis of printed silver electrodes in a microfluidic device, J. Electrochem. Soc 158 (2011) A154, 10.1149/1.3525274.

[88]. Higgins PB, Shade RE, Rodríguez-Sánchez IP, Garcia-Forey M, Tejero ME, Voruganti VS, Cole S.a., Comuzzie AG, Folli F, Central GIP signaling stimulates peripheral GIP release and promotes insulin and pancreatic polypeptide secretion in nonhuman primates, Am. J. Physiol. Metab 311 (2016) E661–E670, 10.1152/ajpendo.00166.2016.

[89]. W.P. Instruments, Aladdin Programmable Syringe Pump, (2010) https://www.idex-hs.com/store/fluidics/valves/flow-regulating-valves/4-way-peek-valves/4-way-flow-valve-peek.html?optionvalue=6623x.

[90]. Yu F, Horowitz M.a., Quake SR, Microfluidic serial digital to analog pressure converter for arbitrary pressure generation and contamination-free flow control, Lab Chip 13 (2013) 1911, 10.1039/c3lc41394b. [PubMed: 23529280]

[91]. Gong H, Woolley AT, Nordin GP, High density 3D printed microfluidic valves, pumps, and multiplexers, Lab Chip 16 (2016) 2450–2458, 10.1039/C6LC00565A. [PubMed: 27242064]

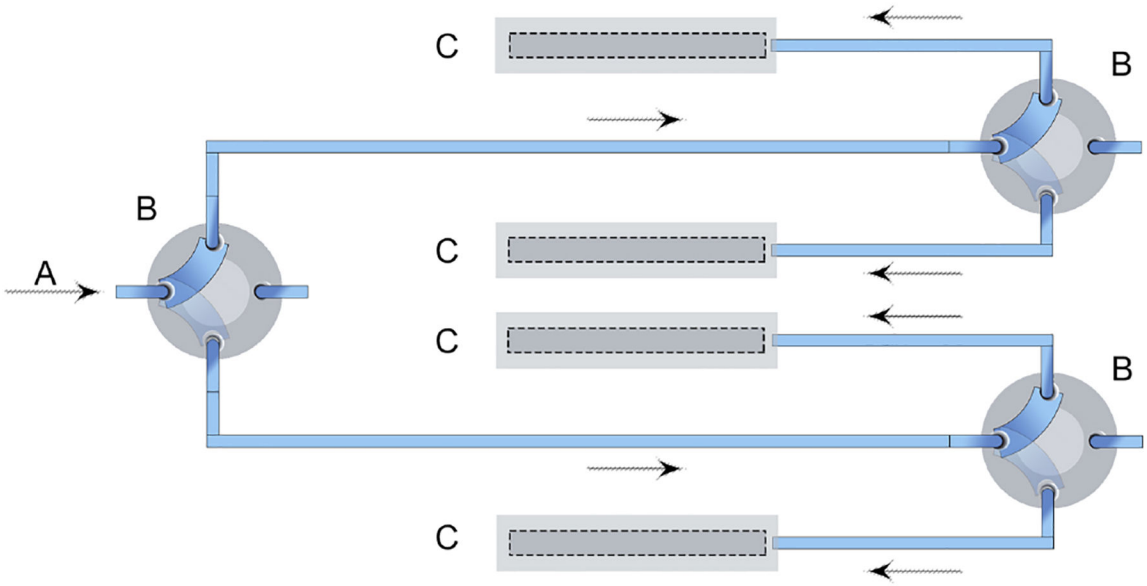

Fig. 1.

Simplified schematic of automated microfluidic system: (A) syringe pump and sample injector, (B) servo-valve, (C) electrochemical detection chamber.

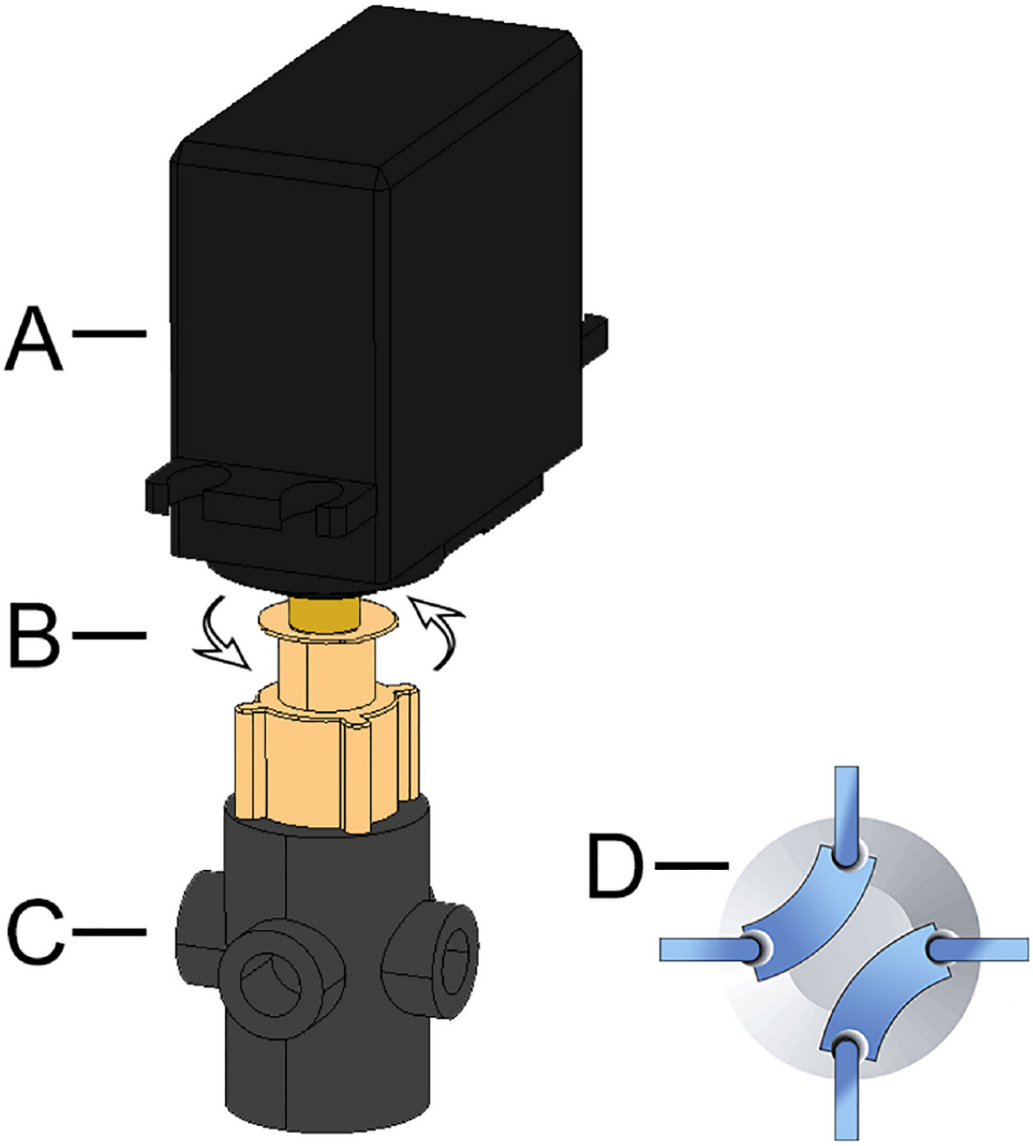

Fig. 2.
Diagram of a configured servo-valve: (A) servo, (B) 180° rotation, (C) valve, (D) flow path options.

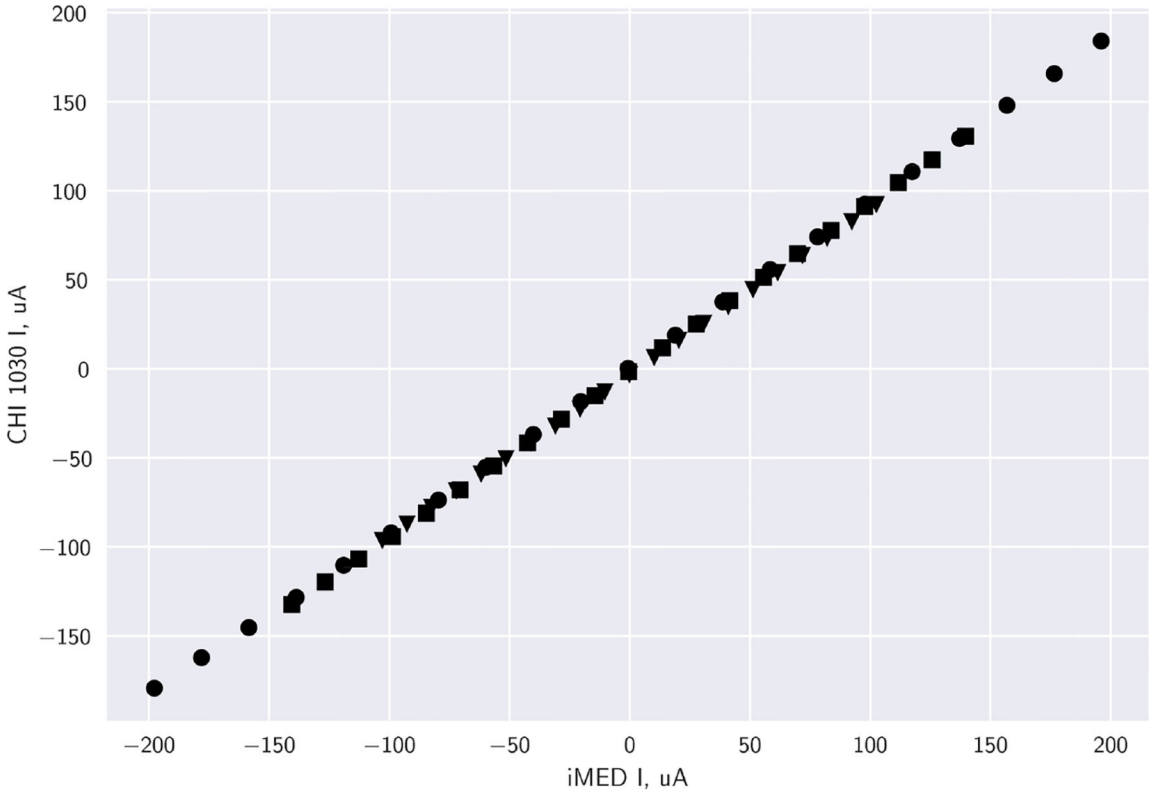

Fig. 3.

Resistor polarization plots of various resistors comparing commercial CHI 1030 and the iMED (averaged $n = 4$): 5.1 kΩ (●), 7.1 kΩ (■), 10 kΩ (▲). Data represents a 2 V potential window, with increments of 0.1 V.

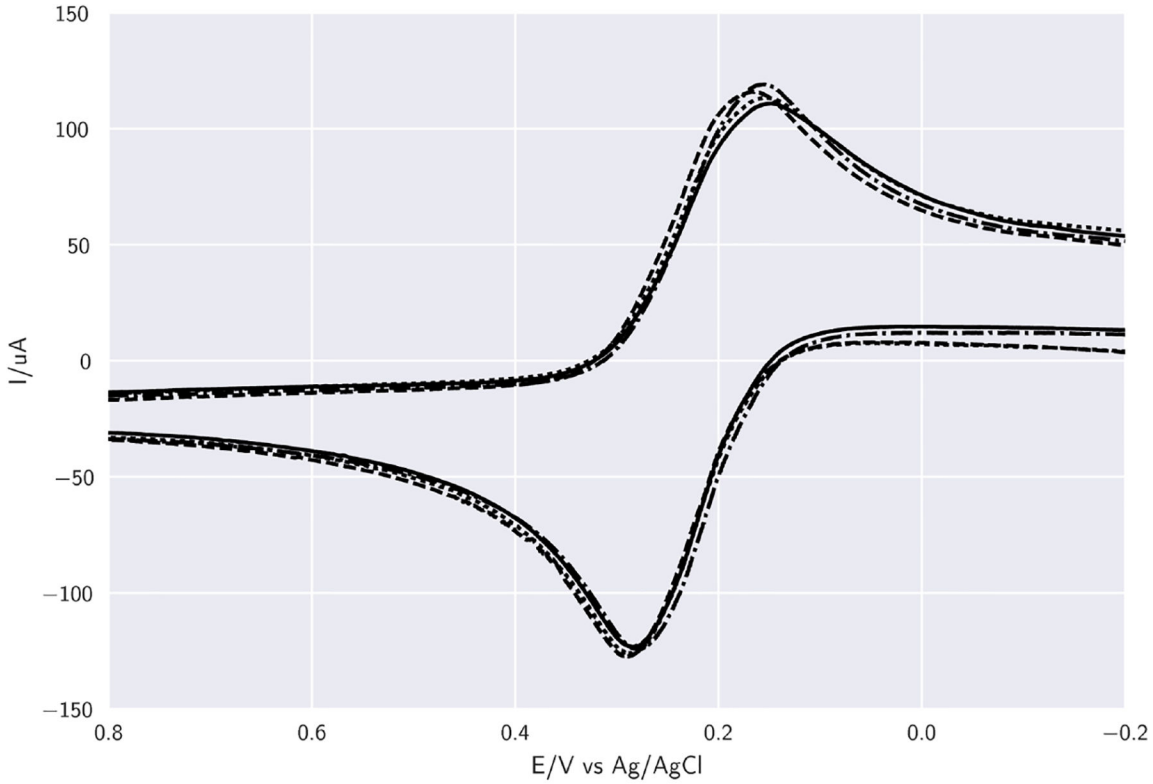

Fig. 4.

Cyclic voltammogram plots of $K_3[Fe(CN)_6]$ comparing 4 channels of the iMED at 100 mV s^{-1}: channel 1 —, channel 2 (- - -), channel 3 (·····), channel 4 (- · -·). Plotted data corresponds to an 8 point moving average using a 1.6 mm platinum working electrode, a 3 M KCl Ag/AgCl reference electrode and a platinum wire counter electrode.

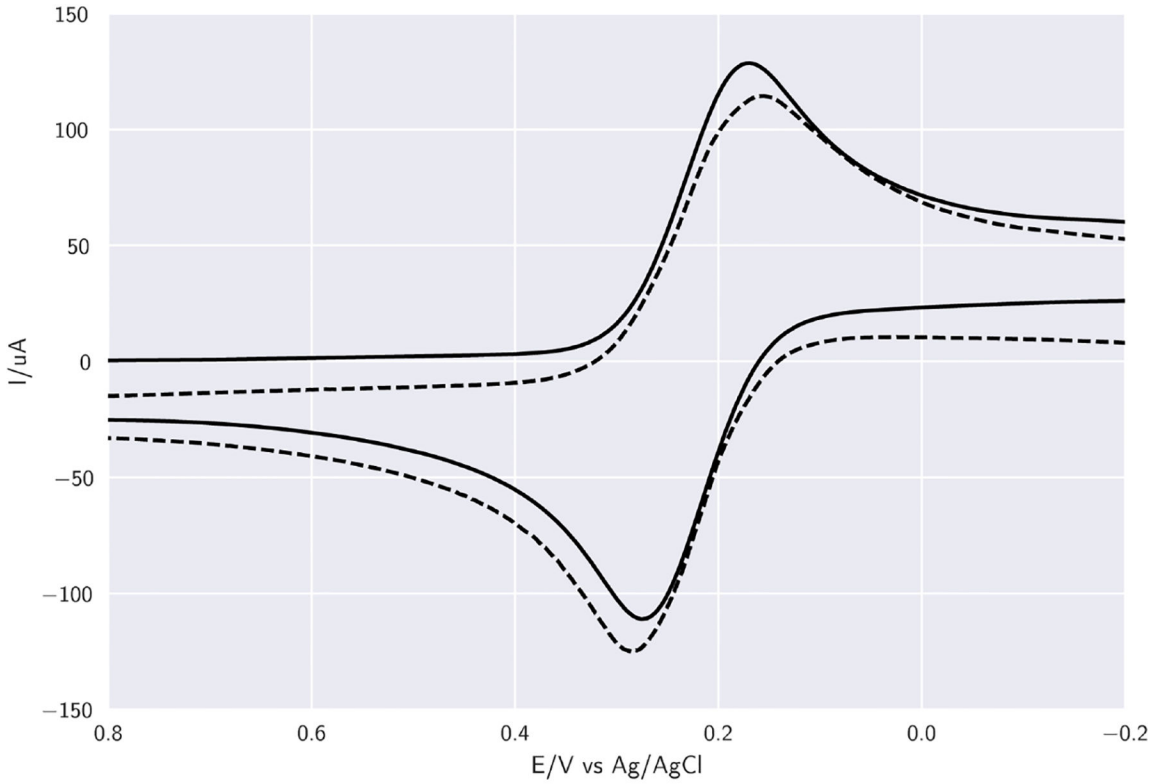

Fig. 5.

Cyclic voltammogram plots of $K_3[Fe(CN)_6]$ comparing 4 channels (averaged $n = 4$), of both the CHI 1030 and iMED, at 100 mV s^{-1}: CHI 1030 (—), iMED (- - -). Plotted data corresponds to an 8 point moving average using a 1.6 mm platinum working electrode, a 3 M KCl Ag/AgCl reference electrode and a platinum wire counter electrode.

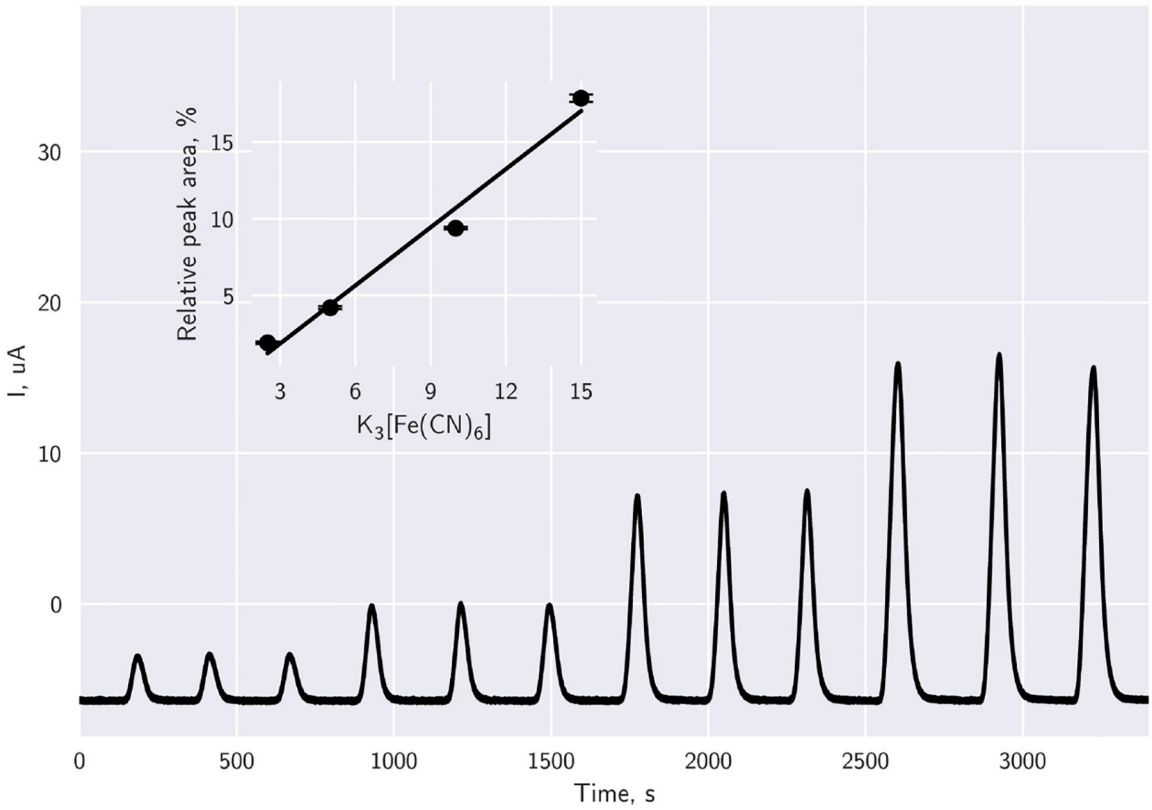

Fig. 6.

Plotted data corresponds to an 8 point moving average of amperometric evaluation of flowing (100 μL min^{-1}) $K_3[Fe(CN)_6]$ using bare Kanichi electrode array at 0.4 V (vs. Ag/AgCl) pseudo-reference in PBS buffer (pH 7.4). Peaks indicate concentrations of $K_3[Fe(CN)_6]$ (2.5, 5, 10, 15 mM) sequentially in triplicate. Inset indicates plotted concentration vs relative peak area response where circles indicate mean peak area values from the evaluations carried out, and error bars indicate the standard deviation ($n = 4$), $y = 1.26162x - 1.9174$ $R^2 = 0.98$.

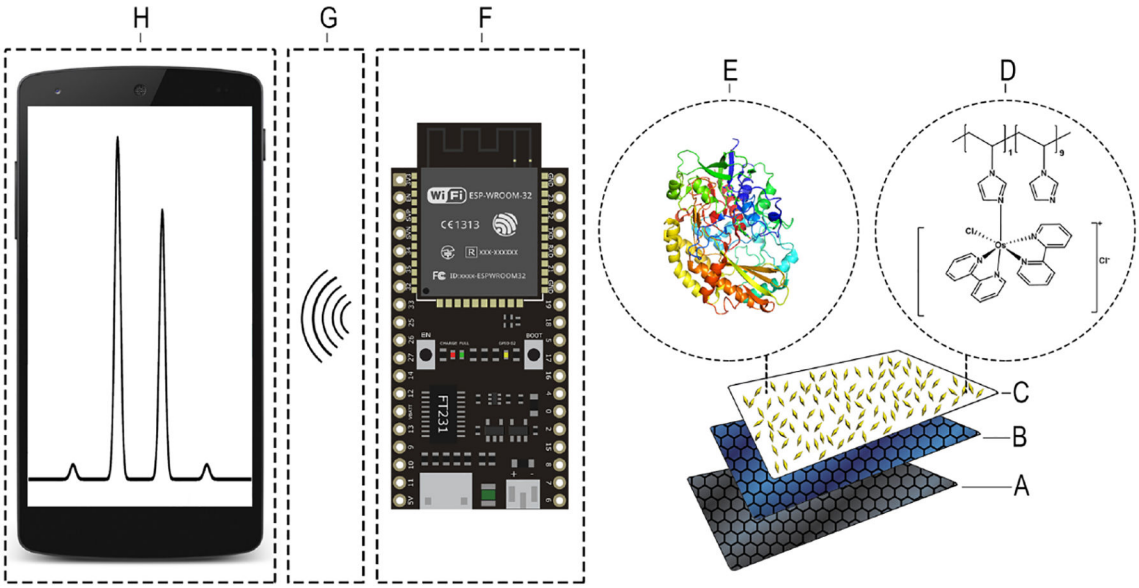

Fig. 7.

Simplified schematic of automated microfluidic wireless potentiostat system: (A) carbon electrode, (B) PEGDGE, (C) MWCNTs, (D) Os(bpy)PVI, (E) FADGDH, (F) wireless potentiostat, (G) wireless data transfer to internet based server, (H) data viewed using internet connected smart phone.

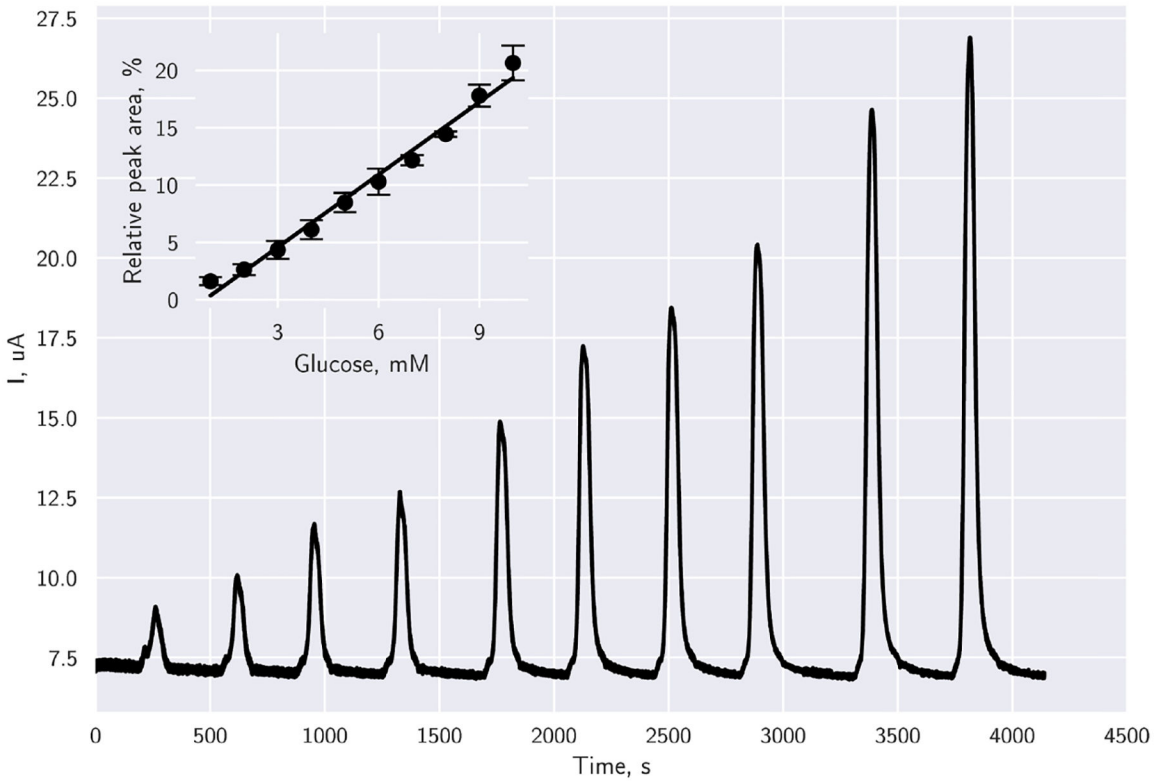

Fig. 8.

Plotted data corresponds to an 8 point moving average of amperometric evaluation of the FADGDH immobilized electrode array at 0.4 V (vs. Ag/AgCl) in PBS buffer (pH 7.4) in channel 1 of the iMED. Inset indicates replications on each channel of the iMED, where circles indicate mean peak area values from the evaluations carried out, and error bars indicate the standard deviation ($n = 4$), $y = 2.10887x - 1.7492$, $R^2 = 0.984$.